

Twist of generalized skyrmions and spin vortices in a polariton superfluid

Stefano Donati,^{1,2} Lorenzo Dominici,^{1,*} Galbadrakh Dagvadorj,³ Dario Ballarini,¹ Milena De Giorgi,¹ Alberto Bramati,⁴ Giuseppe Gigli,¹ Yuri G. Rubo,⁵ Marzena Hanna Szymańska,^{6,†} and Daniele Sanvitto¹

¹ CNR NANOTEC, Istituto di Nanotecnologia, 73100 Lecce, Italy

² Istituto Italiano di Tecnologia, Center for Biomolecular Nanotechnologies Lecce, 73010 Arnesano, Italy

³ Department of Physics, University of Warwick, CV4 7AL Coventry, United Kingdom

⁴ Laboratoire Kastler Brossel, Pierre and Marie Curie University, Sorbonne Universités, CNRS, École Normale Supérieure, Paris Sciences et Lettres Research University, Collège de France, F-75005 Paris, France

⁵ Instituto de Energías Renovables, Universidad Nacional Autónoma de México, Temixco, Morelos 62580, Mexico

⁶ Department of Physics and Astronomy, University College London, WC1E 6BT London, United Kingdom

We study the spin vortices and skyrmions coherently imprinted into an exciton-polariton condensate on a planar semiconductor microcavity. We demonstrate that the presence of a polarization anisotropy can induce a complex dynamics of these structured topologies, leading to the twist of their circuitation on the Poincaré sphere of polarizations. The theoretical description of the results carries the concept of generalized quantum vortices in two-component superfluids, which are conformal with polarization loops around an arbitrary axis in the pseudospin space.

quantum vortices — topology — Poincaré space — condensates — polaritons

Topological defects represent a wide class of objects relevant to different fields of physics from condensed matter to cosmology. The universality of monopoles, vortices, skyrmions, domain walls, and of their formation processes in different systems, has largely motivated their study in the condensed matter context. In particular, the interplay between the symmetry breaking in phase transitions and the formation of topological defects has been the focus of intensive research in the last century. In high energy physics, the existence of an isolated point source intrigued a great number of physicists (1). Dirac was “surprised if Nature had made no use of it” and postulated the possibility of the magnetic monopoles linked to the quantization of electric charge (2). However the elusiveness of their observation in free space has motivated an extensive study of monopole analogues in the form of quasiparticles in many-body systems (3) such as the exotic spin ices (4, 5), liquid crystals (6), exciton-polariton (7) and rubidium Bose-Einstein condensates (BECs) (8, 9), as well as other systems (10, 11). In a 2D multicomponent BEC, an equivalent topological structure to the monopole is given by the hedgehog polarization vortex (12) which together with the hyperspin vortex (13) belong to the class of spin

vortices than when combined lead to a well defined polarization pattern. Such topological states are characterized by a linear polarization vector which rotates an integer number of times (spin winding number) around a singular central point, in a way analogue to what the magnetization does in the spin vortices of a ferromagnetic spinor BEC (14).

In this work we excite complex vortex states in an exciton-polariton superfluid and study their amplitude, phase and polarization dynamics. We demonstrate that temporal evolution of such topologies leads, in general, to a twist of the polarization plane in the Poincaré space. The observed features of the vortex behavior are explained within the concept of generalized spin vortices, where the rotation of polarization at large distances occurs around an arbitrary axis on the Poincaré sphere.

Polaritons emerge in planar semiconductor microcavities as eigenmodes of the strong coupling regime between the exciton resonance and the photon cavity mode, combining the properties of light and matter. The photons confer on polaritons a very small effective mass ($10^{-4} - 10^{-5}$ of free-electron mass) which, together with nonlinear interactions due to the excitons, leads to effective condensation at a relatively high temperature (up to room temperature for given materials such as ZnO, GaN or organic dyes). Features related to superfluidity have been observed such as the suppression of scattering from defects (zero viscosity) (15, 16) or persistence of vortex currents (17). Moreover, polaritons with the pseudospin, given by the possibility of polarizing their state, open the opportunity to study condensates with an internal angular momentum degree of freedom, easily detected by optical means thanks to their photonic outcoupling features (18).

In spinor superfluids, the spin degrees of freedom allow for different composite topologies which emerge as the superposition of quantized vortex states. In superfluids with unrestricted geometry, these elementary vortex blocks are half-quantum vortices (HQVs) (3). In exciton-polariton condensates, the HQV is characterized by a π phase rotation accompanied by a π linear polarization rotation in such an elegant way that the two combine together to ensure the global continuity of the spinor wave function (19–22). For finite-size conden-

*Electronic address: lorenzo.dominici@gmail.com

†Electronic address: m.szymanska@ucl.ac.uk

sates, where the boundary condition at large distances is not fixed, a HQV can be transformed into a skyrmion. The skyrmions possess a specific circumference of full linear polarization and they are fingerprinted by the inversion of the sign of circular polarization degree when crossing this circumference in the radial direction.

On the other hand, the dynamics of the pseudospin vector in semiconductor microcavities is related to the presence of spin-orbital-like coupling, namely, the transverse-electric–transverse-magnetic (TE-TM) splitting of the modes, which is manifested by the optical spin Hall effect (23–25). The TE-TM splitting is often represented by means of an effective magnetic field that produces a precession of the pseudospin vector, which leads to different sectors in circularly polarized states both for real and momentum space, even when starting with a homogeneously polarized field (26, 27).

Here we are able to initialize the polariton condensate with non-trivial pseudospin patterns. We study the dynamics of exotic topologies such as the lemon and the star skyrmion, the hedgehog and the hyperspin vortex, in clean regions of the sample, deriving universal observations not linked to specific local disorder/defects pinning (13) or to the effect of sample architecture/confinement (28). The resultant topologies allow to extend the concept of quantum vortices into a wider class which includes states as generalized skyrmions and spin vortices. These observations subtend the potentialities of resonant excitation of spin and orbital angular momentum states on microcavity polariton fluids, and of their full control using TE-TM or anisotropy splitting, which is of fundamental importance in the field of spintronics and polarization shaping.

Setting up skyrmions and spin vortices

Advanced phase-shaping was recently obtained by means of anisotropic and inhomogeneous liquid-crystal devices called q -plates (29), which allows an extensive investigation of optical vorticity and of full- and half-quantum vortex dynamics in polariton condensates (22). Phase-shaping is applied to an initial Laguerre-Gauss LG_{00} laser pulse (4 ps duration and 0.5 nm bandwidth) by sending it across the q -plate carrying unitary topological charge. The LG_{00} is hence partially or completely transformed into a unitary winding state breaking the chiral symmetry between the two spin populations. Upon proper setting of the incoming/outgoing polarization and tuning of the q -plate, we can prepare the specific combination and resultant field pattern (see [Supporting Information](#) for experimental details). Indeed, each skyrmion and spin vortex shown here can be thought as a composite state resulting from the specific superposition of two LG beams with integer phase winding ($LG_{0,-1/0/+1}$), one in each of the two spin components.

Projected onto the circular polarization basis, the skyrmions are characterized by the presence of an inte-

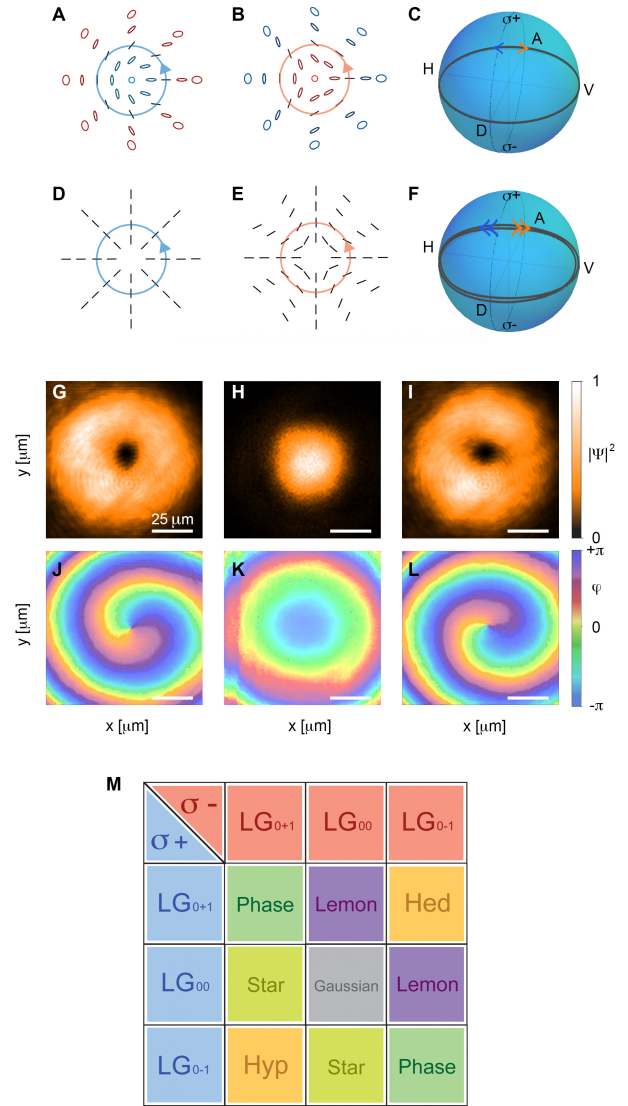


Fig. 1: Generation of vortices. Polarization fields map in real space relating to skyrmion (A,B) and spin (D,E) vortices. The skyrmion cover all the polarization states (full Poincaré patterns), giving rise to lemon-like (A) and star-like (B) patterns. Hedgehog (D) and hyperspin (E) feature a linear polarization in the whole space, following the radial direction and a hyperbolic pattern, respectively. The circles in the real space maps (which represent the l -line in the case of the skyrmions) correspond to the equatorial line in the polarization spheres, with the associated direction for the different states. The colors in the polarization field maps, blue and red, are associated to either the σ_+ (R, right) or σ_- (L, left) degree of circular polarization, respectively, while black is associated to the linear polarization. (C,F) Conformal mapping onto the Poincaré sphere of the real-space circle line around the vortex cores. Spin vortices follow a double rotation in the Poincaré space, skyrmions a single one. (G-I) Experimental initial Laguerre-Gauss states of the polariton population with (J-L) the associated phase maps. Respectively, LG_{0-1} (G,J), LG_{00} (H,K) and LG_{0+1} (I,L). (M) The table summarizes all the possible combinations of LG s in the two cross spin polarizations of the system leading to the different states of quantum vortices: phase vortices (also known as full-vortices), hedgehog (Hed), hyperspin (Hyp), lemon and star skyrmions.

ger phase winding (orbital angular momentum) in one of the spin components and a zero-winding in the opposite one. The resultant vectorial field exhibits an inhomogeneous pattern comprising all polarization states, as typical of full Poincaré beams. There exists a circle line in real-space featuring linear polarization states (l -line, at $r = r_l$), which maps to the equatorial loop of the Poincaré sphere (Fig. 1C). The points inside or outside of the circle are associated with either one or the other hemisphere of the sphere. According to the skyrmion definition, the pseudospin vector flips from right-circular at the core to left-circular (or viceversa) at its boundary ($r \approx 2r_l$). Hence, the real-space radius maps to a given meridian on the sphere, and the meridian angle is then associated to the azimuthal real-space angle. The skyrmion polarization field in the region $r < r_l$ covers only one hemisphere of the Poincaré sphere, and it can be mapped to the polarization field of an infinite-size HQV (19). Therefore, similarly to the HQVs (12), the skyrmions can be characterized by two distinct geometries: lemon-like (Fig. 1A) and star-like (Fig. 1B) skyrmions.

In a spin vortex, the two spin components feature counter-rotating phase windings (see Fig. 1D,E) (13). The central phase singularities in the two spin populations convert into a polarization singularity at the core. There are two principal types of polarization vortices: the hedgehog with a purely radial direction of polarization (Fig. 1D) and the hyperspin vortex, characterized by a hyperbolic polarization pattern (Fig. 1E). Upon changing the phase delay between the two spins, the hedgehog can transform into an azimuthal polarization pattern, while the hyperspin undergoes a texture rotation. These vortex states can be described by an equivalent form when conformally mapping them to points on the Poincaré sphere: the circulation along every circle centered at the vortex core in the real-space can be associated with a closed double loop lying in the equatorial plane (Fig. 1F) of the pseudospin space. In order to make the classification clearer, in the third and fourth rows of Fig. 1 we show examples of the density and phase profiles of the fundamental building blocks of all type of vortices in circular polarization basis: clockwise LG_{0-1} (G,J), zero-winding LG_{00} (H,K) and counter-clockwise LG_{0+1} (I,L) states. Different combinations of the three LGs in the two circular polarizations σ_+ and σ_- (the two opposite pseudospins) leading to skyrmion, spin and phase vortices are shown in Fig. 1M.

These photonic states are set as the initial conditions of the polaritonic population dynamics by resonant excitation on the microcavity sample, at the energy of the lower polariton branch (LPB). On the detection side, we extract both the instantaneous local density and the phase of the polariton emission during its time evolution, by means of an interferometric setup performing real-time digital Fourier transform and off-axis selection (30–32). Using polarization filtering in detection, we can project the single components in each of the

three polarization basis, the linear horizontal-vertical (H - V), diagonal-antidiagonal (D - A) and the circular right-left (R - L). From these measurements it is possible to retrieve the full map of the different degrees of polarization, and Stokes parameters $S_{1,2,3}$, respectively, which are used to plot the resultant polarization vector field, and to associate every point in real-space to the pseudospin space (33) (see [Supporting Information](#)).

Twist of the vortex polarization field

The variation of the $S_{1,2,3}$ parameters in real-space for the hyperspin polarization vortex is presented in the first row of Fig. 2 (A-C). These plots relate to the emission from the polariton condensate at the initial time (after the laser pulse has arrived), and the degrees of polarizations are clearly mapped also in the regions of weak or null intensity, such as in the centre of a vortex. The twofold symmetry (C_2 symmetry) of the S_1 (Fig. 2A) and S_2 (Fig. 2B) results in a petal shape of the polarization distribution, while S_3 is approximately zero over all space as expected. The presence of a very small component in the S_3 can be attributed to the q -plate device, which cannot be simultaneously tuned at all the wavelengths composing the pulsed beam. However, the circular degree of polarization is far weaker than the linear components of the S_1 and S_2 parameters.

The most pronounced effect appears in the time evolution of the spin degree: the S_3 component increases during the system evolution, becoming almost as large as the linear degree of polarization. This effect is clearly visible in Fig. 2D, where we show the azimuthal profile of S_3 (taken along the gray circle in Fig. 2C) whose sinusoidal modulation increases with time. Similar dynamics are observed also when starting with a skyrmion state. Fig. 2E-G shows, for the skyrmion configuration, the associated $S_{1,2,3}$ maps with a lowered symmetry in the S_1 and S_2 linear degrees and a concentric distribution for S_3 , which changes from -1 to $+1$ from the centre outwards. We plot the azimuthal profile of S_3 along the l -line of purely linear polarizations (gray circle in panel G), at different times, in Fig. 2H (see also [Movie S1](#)). Although the circular degree of polarization is approximately zero at the initial time, during time evolution an increasing imbalance of right and left spin polarizations develops. Also, in this skyrmion case, the profile assumes a sinusoidal modulation growing in amplitude, and rising even larger than in the case of the polarization vortices. We checked that this effect is not due to a real-space movement of the whole topological state with respect to the initial circle. Indeed the phase singularities (vortex cores), that can be tracked for each spin component possessing a nonzero phase winding (either two phase singularities for the polarization vortices, or one for the skyrmions), remain quite stable during the whole dynamics with just a few μm displacement even after 45 ps (see also [Movie S2](#)).

The same effects are observed when starting with a hedgehog vortex and with a star skyrmion. In par-

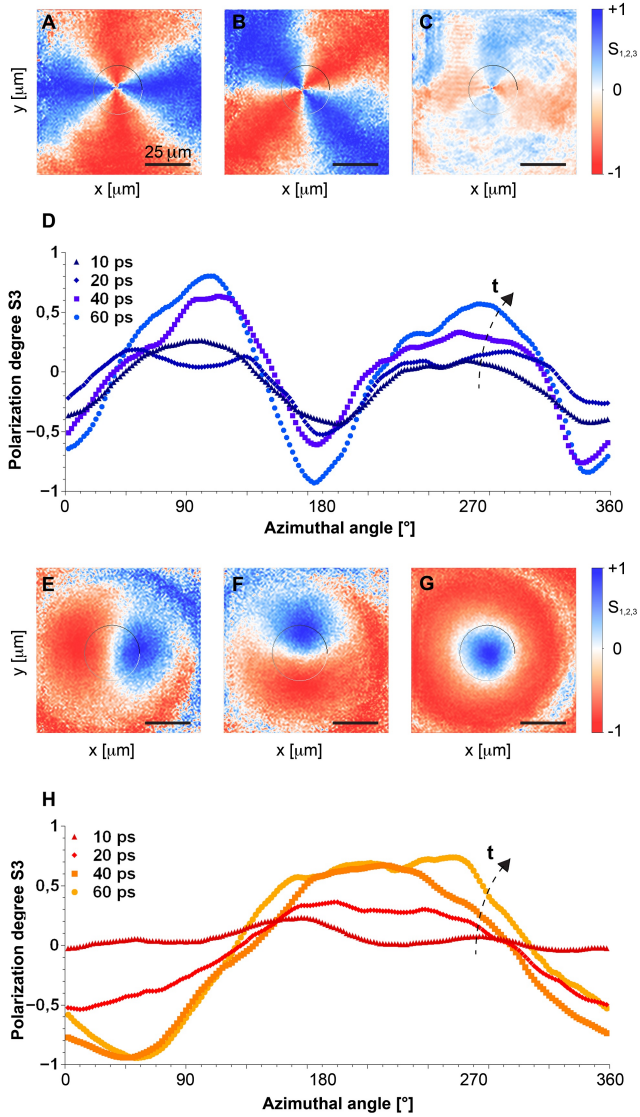


Fig. 2: Stokes maps. (A-C) Polarization maps of the polariton hyperspin vortex at the initial time, given as a projection onto the three Stokes basis, horizontal-vertical (S_1 , A) diagonal-antidiagonal (S_2 , B) and circular right-left (S_3 , C). (D) Time evolution of the circular degree of polarization, plotted as S_3 angular profiles around the vortex core at different times. (E-G) S_1 , S_2 and S_3 maps of the lemon-like skyrmion at initial time and (H) associated time evolution of the spin degree profile S_3 . All the profiles have been taken along the black/white circle plotted in the real space maps, which represents the l -line of the skyrmion.

ticular, in Fig. 3, we plot the full polarization vectors in real-space, retrieved from the $S_{1,2,3}$ maps. The first row shows the polarization vector for the hedgehog at three different time frames. At the initial time, Fig. 3A, the field pattern follows the classic hedgehog structure schematically introduced in Fig. 1D. The colours used here refer directly to the degree of spin polarization S_3 . In addition, in Fig. 3D, we show the double loop of the

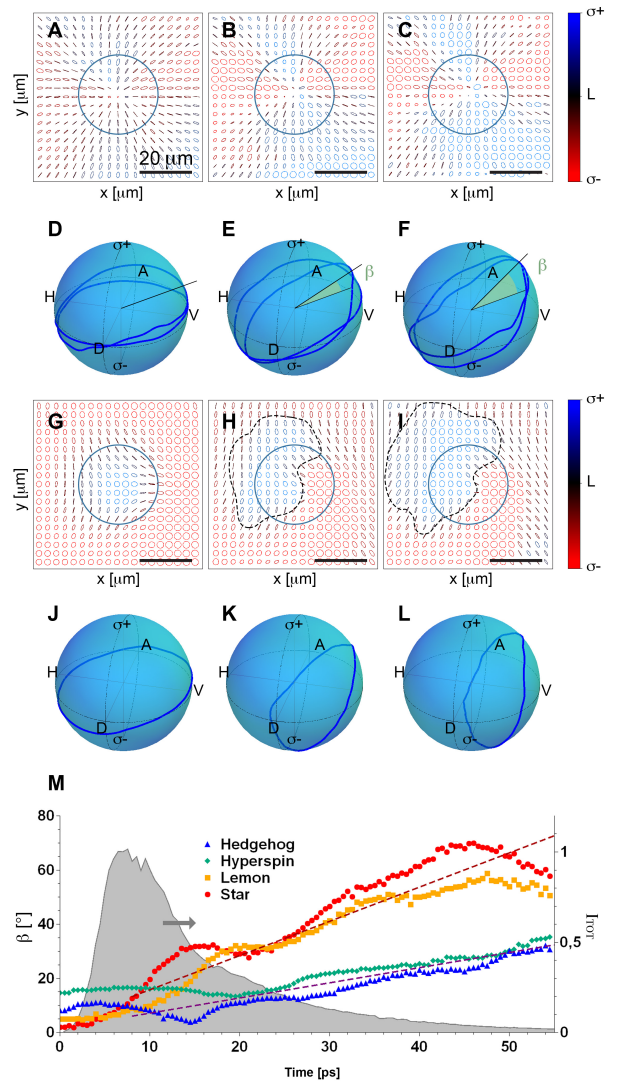


Fig. 3: Polarization textures. (A-C) Experimental polarization textures of the hedgehog vortex at 20, 45, 54 ps and (D-F) conformal mapping onto the Poincaré sphere of the real-space profile (blue solid circle line in the both kind of maps). (G-I) Polarization texture of the star-like skyrmion at 20, 45, 54 ps and (J-L) associated plotting in the Poincaré space. The solid blue circle represents the initial boundary line between σ_+ and σ_- spin domains (l -line), while its evolution at later time is reported as a dashed black line. (M) Twisting dynamics, represented by the angle β between the plane containing the single- and double-loops around the polarization sphere and the equatorial plane as a function of time. The time behavior of the total population (grey shaded area) shows that the twisting dynamics are basically independent on the polariton density (straight dashed lines are just a guide for the eye).

pseudospin along the Poincaré sphere. The subsequent dynamics are presented as vector maps in Fig. 3B,C (see also [Movie S3](#)). On the Poincaré sphere, Fig. 3E,F, we observe a clear twist of the plane containing the double loop away from the equatorial plane, where this effect grows in time (see also [Movie S4](#)). The twist angle

β is directly linked to the maximum degree of circular polarization assumed by the polariton population, as $\beta = \max \arcsin S_3$. By sinusoidal fitting of the azimuthal profiles of $S_{1,2,3}$, we retrieve the trajectory and twist angle β of the double loop.

Analogous effects are observed for the star skyrmion, which vector textures are shown in the third row. The experimental map at the initial time, Fig. 3G, is very close to the sketch pattern of Fig. 1B. The polarization reshaping at later times, as shown in Fig. 3H,I, results in an apparent spin transport with respect to the inner circle, initially containing prevalent positive spin (σ_+), both outwards (from the top-left area) and inward (to the bottom-right part). Overall, by considering the sign of the spin, the entering negative currents (σ_-) contribute to the net outgoing positive spin flux. We should emphasize that the spin transport is decoupled from the mass transport and from the phase singularity movement. Yet again, it is possible to clearly follow the dynamics on the Poincaré sphere, as in Fig. 3J-L, where the single-loop initially on the equator undergoes a large twist also for this case. A similar reshaping effect has been observed before for the spontaneous hyperbolic spin vortex generated in non-resonant quasi-cw condition by Manni *et al.* (13). However, in that case the vortex was instead pinned by a defect and the causes for twisting were ascribed to the interplay between the disorder potential and the finite- k TE-TM splitting, relevant due to radial flows of polaritons.

Theory models and discussion

In order to understand the physical origins of our observations, we perform numerical modelling of the system's dynamics using two-component open-dissipative Gross-Pitaevskii equations, which describe the microcavity photon field and the quantum well exciton field coupled to each other. The excitonic coupling between differently polarized populations is usually represented by the inter-spin nonlinearity term (34), although here we are interested in the linear regime. Fundamental to the present work are the terms directly acting on the photonic fields (see [Supporting Information](#) for the model details), as discussed in the following. The photonic coupling between different polarizations is given by the finite- k TE-TM splitting term χ and the k -independent anisotropy splitting χ_0 . The former appears due to the difference of transverse-electric and transverse-magnetic masses of microcavity modes (35), while the k -independent splitting χ_0 between linearly polarized modes can be present in some samples due to strain effects (36, 37) and heavy-light hole mixing (38) on the quantum well interfaces. In such cases two linearly polarized waves with specific polarization directions (say, x and y), are subject to a slight different energy shift, regardless of the direction and of their wavevector. Hence, also the $k = 0$ state can be subject to a dephasing between the two linear components, and as a result there could be a precession of an initial polariza-

tion state (different from the linear x and y ones) at each point in space.

To reproduce the polarization twisting observed in our experiment we perform different sets of simulations. In the first set we take the k -independent anisotropy splitting χ_0 to be zero, and in the second set we assume it to be in the $\chi_0 = 0.01 \text{ meV} - 0.04 \text{ meV}$ range, estimated on the basis of polarization resolved photoluminescence. We see no twist effect in the dynamics when $\chi_0 = 0$, and instead see a significant twist, comparable to experimental, in the simulations with χ_0 inside the said range (Fig. 4). The initial $S_{1,2,3}$ Stokes maps for the spin vortices are reported in Fig. 4A-C, respectively, for the case of a hedgehog state. Here the initial degree of circular polarization is homogeneously null (S_3 map of panel C). The evolution of $S_{1,2,3}$ at later times ($t = 67 \text{ ps}$), presented in the second row of Fig. 4D-F, shows emergence of a strong circular polarization under the action of a $\chi_0 \equiv \chi_{02} = 0.02 \text{ meV}$. The S_3 map (panel F) exhibits a symmetric division in four quadrants aligned as those of the S_2 parameter (panel E). S_2 is maintaining the same orientation as in the initial state but is decreasing in its intensity, while the S_1 is essentially unmodified in both orientations and intensity. This effect is indeed observed only in the presence of a $k = 0$ xy anisotropy, which in the simulations has the specific orientation along the x and y axis and thus is not affecting the S_1 pattern. On the Poincaré sphere, the space circulation of the polarization vortices around the cores at the initial time can be mapped to a double rotation on the sphere lying in the equatorial plane as in Fig. 4M. The effect of the dynamical polarization reshaping is equivalent to a twist of the geodesics around the S_1 axis towards the circular poles, which grows in time.

Similar effects are observed when starting with a skyrmion. As an example in Fig. 4G-I we show the star-like state, with their associated two-sector symmetry in the linear polarizations. Here the degree of circular polarization is not zero at the initial state due to the skyrmion structure, which translates to a vortex in one circular polarization and the Gaussian state in the other. The polarization evolves in time in a similar way to what we have seen for the skyrmions in the experiment, and is caused by the mechanism associated with the χ_0 splitting, as described earlier. Figure 4J-L shows the Stokes maps obtained at later time ($t = 67 \text{ ps}$) again under the action of a $\chi_0 \equiv \chi_{02}$ anisotropy value. We also examine the polarization profile along a circle in real space taken along the so called l -line, marked on the maps as a black solid circle. This is conformal to a single loop around the equator of the Poincaré sphere as shown the Fig. 4N. Here we report the loops at fixed time ($t = 55 \text{ ps}$) and for different increasing χ_0 values ($\chi_{01} = 0.01 \text{ meV}$, $\chi_{02} = 0.02 \text{ meV}$, $\chi_{03} = 0.03 \text{ meV}$, $\chi_{04} = 0.04 \text{ meV}$). The polarization reshaping with its associated Stokes twist is once again happening along the S_1 axis and it is proportional to the χ_0 strength (see also [Movie S5](#)). The initially circular symmetry of

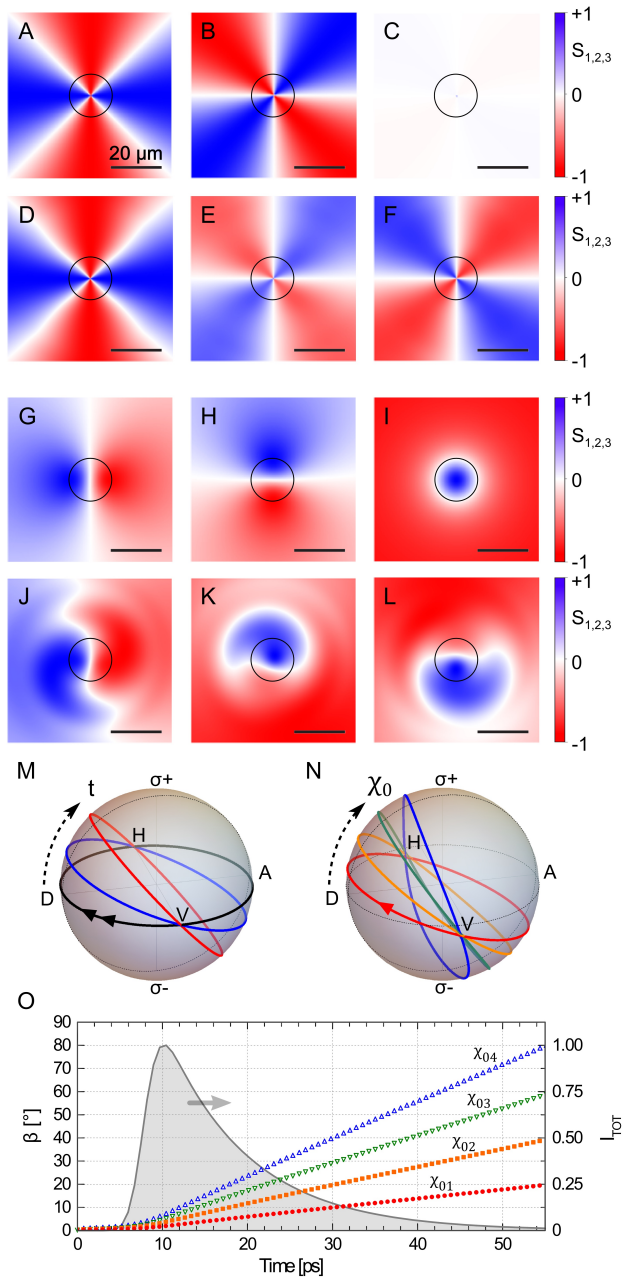


Fig. 4: Theoretical analysis. (A-C) Polarization maps of the hedgehog vortex from numerical simulations at the early stage and (D-F) final time ($t = 67$ ps). (G-I) S_1 , S_2 and S_3 maps of the star-like skyrmion at initial and (J-L) final time ($t = 67$ ps). (M-N) Twisting of the associated double-loop (M) and single-loop (N) trajectory in the Poincaré sphere, retrieved along the black circle in the real space maps (which is the initial l -line of the skyrmion). In panel M the loops are traced at different times ($t = 6$ ps, 34 ps and 67 ps) and constant anisotropy ($\chi_0 \equiv \chi_{02}$), while in N the loops are traced at fixed time ($t = 55$ ps) and different χ_0 values ($\chi_{01} = 0.01$ meV, $\chi_{02} = 0.02$ meV, $\chi_{03} = 0.03$ meV, $\chi_{04} = 0.04$ meV) (O) Time evolution of the twist angle β for the same anisotropy values used in panel N. The twist rate is constant in time and linear on the χ_0 value, and independent on the topology state (which is, each $\beta(t)$ twist curve in the panel O is for the same anisotropy values, hedgehog and hyperspin, lemon and star skyrmion).

the spin degree in real space evolves as well, as seen in Fig. 4L. It assumes a distribution which is somehow complementary to that of the S_2 one.

Conclusions and Perspectives

In summary, the dephasing of x and y linear polarization components, leads to a transformation of the diagonal-antidiagonal degree of polarization into a circular spin degree, for both spin vortices and skyrmions. By comparing with the experiments, we deduce that the axis of the $k = 0$ splitting anisotropy in our experimental configurations are oriented along the diagonal and antidiagonal directions. The twist speed induced by the χ_0 term in the simulations is the same for all four considered states. The perfectly linear trend in time (starting from $t = 8$ ps, that is when the fluid is left free to evolve after the arrival of the exciting pulse) shown in Fig. 4O demonstrates the effect to be independent of the instantaneous density of polaritons, which decay according to the $\tau_{\text{LP}} = 10$ ps. On the other hand the strength of the twist is directly proportional to the anisotropy value, as demonstrated by looking at the slopes of the β curves in Fig. 4O corresponding to different χ_0 . We can evaluate a theoretical twist speed of $\sim 40^\circ(\text{ps} \cdot \text{meV})^{-1}$. Noticeably here (for the skyrmions), we also observe an interesting evolution of the S_1 pattern in real space (Fig. 4J). There is a sort of rotation of the sectors with some features of spiralling. This additional effect, i.e., the rotations of the $S_{1,2,3}$ sectors in real space, is instead associated to the action of the finite- k TE-TM splitting term χ in our model (27). We would like to stress that our simulations clearly confirm that it is the xy anisotropy, which is the cause for the polarization twisting of vortex states. On the contrary, the disorder potential term, produced by the inhomogeneities inside the cavity mirror, was not needed to reproduce the observed dynamics.

From a theoretical point of view, the reshaping of the polarization field, and more specifically their Stokes twist, can be a convenient way to define the generalized quantum vortex, where the angle β measures the inclination between the plane of polarization rotation and the equatorial plane in the Poincaré sphere. We note that the concept of generalized quantum vortex can be used to describe the new type of half-quantum circulation, recently found in a macroscopic ring by Liu *et al.* (39) under non-resonant pulsed pumping. Namely, this vortex corresponds to the polarization rotation around a tilted axis on the pseudospin sphere. We can hence define the generalized skyrmion as a full Poincaré topology which real-space circulations are conformal to a family of single loop curves around an arbitrary axis on the pseudospin sphere (see [Movie S6](#)). The same concept can apply to the spin vortices, whose generalized version maps to a double loop along an arbitrary great circle of the Poincaré sphere.

Methods summary

The experimental polariton device is a typical photonic

microcavity (MC) embedding quantum wells (QW) kept at cryogenic temperature. A ps laser pulse tuned on the lower polariton branch energy works as the excitation and reference beams. Optical vortices and their composition are obtained by means of a liquid crystal q -plate device, waveplates and polarizers. Space-temporal dynamics are retrieved upon implementing the off-axis digital holography technique on a custom interferometric setup. The modelling of the system is based on coupled two-component open-dissipative Gross-Pitaevskii equations for the MC photons and QW excitons. Dynamical simulations of the equations are implemented on the XMDS2 software framework (40). For experimental and

theoretical details see refs. (22, 30), and (33) and [Supporting Information](#).

ACKNOWLEDGEMENTS. We thank R. Houdré for the microcavity sample and L. Marrucci and B. Piccirillo for the q -plate devices. This work was supported by European Research Council POLAFLOW Grant 308136, Italian Ministero dell'Istruzione dell'Università e della Ricerca project "Beyond Nano", Engineering and Physical Sciences Research Council Grants EP/I028900/2 and EP/K003623/2 (to M.H.S.), and Consejo Nacional de Ciencia y Tecnología Grant 251808 (to Y.G.R.).

-
- [1] Y. M. Shnir, *Magnetic Monopoles* (Springer-Verlag, Berlin Heidelberg, 2005).
- [2] P. A. M. Dirac, *Quantised singularities in the electromagnetic field*, Proc. R. Soc. Lond. **133** (1931).
- [3] G. E. Volovik, *The Universe in a Helium Droplet* (Oxford University Press, New York, 2003).
- [4] C. Castelnovo, R. Moessner, and S. L. Sondhi, *Magnetic monopoles in spin ice*, Nature **451**, 42 (2008).
- [5] D. J. P. Morris, D. A. Tennant, S. A. Grigera, B. Klemke, C. Castelnovo, R. Moessner, C. Czternasty, M. Meissner, K. C. Rule, J.-U. Hoffmann, K. Kiefer, S. Gerischer, D. Slobinsky, and R. S. Perry, *Dirac strings and magnetic monopoles in the spin ice Dy₂Ti₂O₇*, Science **326**, 411 (2009).
- [6] I. Chuang, R. Durrer, N. Turok, and B. Yurke, *Cosmology in the laboratory: Defect dynamics in liquid crystals*, Science **251**, 1336 (1991).
- [7] R. Hivet, H. Flayac, D. D. Solnyshkov, D. Tanese, T. Boulier, D. Andreoli, E. Giacobino, J. Bloch, A. Bramati, G. Malpuech, and A. Amo, *Half-solitons in a polariton quantum fluid behave like magnetic monopoles*, Nat. Phys. **8**, 724 (2012).
- [8] M. Ray, E. Ruokokoski, S. Kandel, M. Möttönen, and D. Hall, *Observation of Dirac monopoles in a synthetic magnetic field*, Nature **505**, 657 (2014).
- [9] M. W. Ray, E. Ruokokoski, K. Tiurev, M. Möttönen, and D. S. Hall, *Observation of isolated monopoles in a quantum field*, Science **348**, 544 (2015).
- [10] Z. Fang, N. Nagaosa, K. S. Takahashi, A. Asamitsu, R. Mathieu, T. Ogasawara, H. Yamada, M. Kawasaki, Y. Tokura, and K. Terakura, *The anomalous Hall effect and magnetic monopoles in momentum space*, Science **302**, 92 (2003).
- [11] P. Milde, D. Köhler, J. Seidel, L. M. Eng, A. Bauer, A. Chacon, J. Kindervater, S. Mühlbauer, C. Pfleiderer, S. Buhrandt, C. Schütte, and A. Rosch, *Unwinding of a skyrmion lattice by magnetic monopoles*, Science **340**, 1076 (2013).
- [12] M. Toledo-Solano, M. E. Mora-Ramos, A. Figueroa, and Y. G. Rubo, *Warping and interactions of vortices in exciton-polariton condensates*, Phys. Rev. B **89**, 035308 (2014).
- [13] F. Manni, Y. Léger, Y. G. Rubo, R. André, and B. Deveaud, *Hyperbolic spin vortices and textures in exciton-polariton condensates*, Nat. Commun. **4** (2013).
- [14] L. Sadler, J. Higbie, S. Leslie, M. Vengalattore, and D. Stamper-Kurn, *Spontaneous symmetry breaking in a quenched ferromagnetic spinor Bose-Einstein condensate*, Nature **443**, 312 (2006).
- [15] A. Amo, D. Sanvitto, F. P. Laussy, D. Ballarini, E. del Valle, M. D. Martin, A. Lemaître, J. Bloch, D. N. Krizhanovskii, M. S. Skolnick, C. Tejedor, and L. Viña, *Collective fluid dynamics of a polariton condensate in a semiconductor microcavity*, Nature **457**, 291 (2009).
- [16] A. Amo, J. Lefrère, S. Pigeon, C. Adrados, C. Ciuti, I. Carusotto, R. Houdré, E. Giacobino, and A. Bramati, *Superfluidity of polaritons in semiconductor microcavities*, Nat. Phys. **5**, 805 (2009).
- [17] D. Sanvitto, F. M. Marchetti, M. H. Szymańska, G. Tosi, M. Baudisch, F. P. Laussy, D. N. Krizhanovskii, M. S. Skolnick, L. Marrucci, A. Lemaître, J. Bloch, C. Tejedor, and L. Viña, *Persistent currents and quantized vortices in a polariton superfluid*, Nat. Phys. **6**, 527 (2010).
- [18] I. A. Shelykh, A. V. Kavokin, Y. G. Rubo, T. C. H. Liew, and G. Malpuech, *Polariton polarization-sensitive phenomena in planar semiconductor microcavities*, Semicond. Sci. Technol. **25**, 013001 (2010).
- [19] Y. G. Rubo, *Half vortices in exciton polariton condensates*, Phys. Rev. Lett. **99**, 106401 (2007).
- [20] K. G. Lagoudakis, T. Ostatnický, A. V. Kavokin, Y. G. Rubo, R. André, and B. Deveaud-Plédran, *Observation of half-quantum vortices in an exciton-polariton condensate*, Science **326**, 974 (2009).
- [21] F. Manni, K. G. Lagoudakis, T. C. H. Liew, R. André, V. Savona, and B. Deveaud, *Dissociation dynamics of singly charged vortices into half-quantum vortex pairs*, Nat. Commun. **3**, 1309 (2012).
- [22] L. Dominici, G. Dagvadorj, J. M. Fellows, D. Ballarini, M. De Giorgi, F. M. Marchetti, B. Piccirillo, L. Marrucci, A. Bramati, G. Gigli, M. H. Szymańska, and D. Sanvitto, *Vortex and half-vortex dynamics in a nonlinear spinor quantum fluid*, Sci. Adv. **1** (2015).
- [23] A. Kavokin, G. Malpuech, and M. Glazov, *Optical spin Hall effect*, Phys. Rev. Lett. **95**, 136601 (2005).
- [24] C. Leyder, M. Romanelli, J. P. Karr, E. Giacobino, T. C. H. Liew, M. M. Glazov, A. V. Kavokin, G. Malpuech, and A. Bramati, *Observation of the optical spin Hall effect*, Nat. Phys. **3**, 628 (2007).
- [25] E. Kammann, T. C. H. Liew, H. Ohadi, P. Cilibrizzi, P. Tsotsis, Z. Hatzopoulos, P. G. Savvidis, A. V. Kavokin, and P. G. Lagoudakis, *Nonlinear optical spin Hall effect and long-range spin transport in polariton lasers*, Phys. Rev. Lett. **109**, 036404 (2012).
- [26] P. Cilibrizzi, H. Sigurdsson, T. C. H. Liew, H. Ohadi, A. Askitopoulos, S. Brodbeck, C. Schneider, I. A. Shelykh, S. Höfling, J. Ruostekoski, and P. Lagoudakis, *Half-*

-
- skyrmion spin textures in polariton microcavities*, Phys. Rev. B **94**, 045315 (2016).
- [27] P. Cilibrizzi, H. Sigurdsson, T. C. H. Liew, H. Ohadi, S. Wilkinson, A. Askitopoulos, I. A. Shelykh, and P. G. Lagoudakis, *Polariton spin whirls*, Phys. Rev. B **92**, 155308 (2015).
- [28] S. Dufferwiel, F. Li, E. Cancellieri, L. Giriunas, A. A. P. Trichet, D. M. Whittaker, P. M. Walker, F. Fras, E. Clarke, J. M. Smith, M. S. Skolnick, and D. N. Krizhanovskii, *Spin textures of exciton-polaritons in a tunable microcavity with large TE-TM splitting*, Phys. Rev. Lett. **115**, 246401 (2015).
- [29] F. Cardano, E. Karimi, S. Slussarenko, L. Marrucci, C. de Lisio, and E. Santamato, *Polarization pattern of vector vortex beams generated by q-plates with different topological charges*, Appl. Opt. **51**, C1 (2012).
- [30] L. Dominici, D. Colas, S. Donati, J. P. Restrepo Cuartas, M. De Giorgi, D. Ballarini, G. Guirales, J. C. López Carreño, A. Bramati, G. Gigli, E. del Valle, F. P. Laussy, and D. Sanvitto, *Ultrafast control and Rabi oscillations of polaritons*, Phys. Rev. Lett. **113**, 226401 (2014).
- [31] C. Antón, G. Tosi, M. D. Martín, L. Viña, A. Lemaître, and J. Bloch, *Role of supercurrents on vortices formation in polariton condensates*, Opt. Express **20**, 16366 (2012).
- [32] G. Nardin, K. G. Lagoudakis, B. Pietka, F. Morier-Genoud, Y. Léger, and B. Deveaud-Plédran, *Selective photoexcitation of confined exciton-polariton vortices*, Phys. Rev. B **82**, 073303 (2010).
- [33] D. Colas, L. Dominici, S. Donati, A. A. Pervishko, T. C. H. Liew, I. A. Shelykh, D. Ballarini, M. de Giorgi, A. Bramati, G. Gigli, E. del Valle, F. P. Laussy, A. V. Kavokin, and D. Sanvitto, *Polarization shaping of Poincaré beams by polariton oscillations*, Light Sci. Appl. **4**, e350 (2015).
- [34] L. Ferrier, E. Wertz, R. Johne, D. D. Solnyshkov, P. Senellart, I. Sagnes, A. Lemaître, G. Malpuech, and J. Bloch, *Interactions in Confined Polariton Condensates*, Phys. Rev. Lett. **106**, 126401 (2011).
- [35] K. Y. Bliokh, F. J. Rodríguez-Fortuño, F. Nori, and A. V. Zayats, *Spin-orbit interactions of light*, Nat. Photon. **9**, 796 (2015).
- [36] R. Balili, B. Nelsen, D. W. Snoke, R. H. Reid, L. Pfeiffer, and K. West, *Huge splitting of polariton states in microcavities under stress*, Phys. Rev. B **81** (2010).
- [37] L. Klopotoski, M. Martín, A. Amo, L. Viña, I. Shelykh, M. Glazov, G. Malpuech, A. Kavokin, and R. André, *Optical anisotropy and pinning of the linear polarization of light in semiconductor microcavities*, Solid State Commun. **139**, 511 (2006).
- [38] E. L. Ivchenko, A. Y. Kaminski, and U. Rössler, *Heavy-light hole mixing at zinc-blende (001) interfaces under normal incidence*, Phys. Rev. B **54**, 5852 (1996).
- [39] G. Liu, D. W. Snoke, A. Daley, L. N. Pfeiffer, and K. West, *A new type of half-quantum circulation in a macroscopic polariton spinor ring condensate*, Proc. Natl. Acad. Sci. **112**, 2676 (2015).
- [40] G. R. Dennis, J. J. Hope, and M. T. Johnsson, *XMDS2: Fast, scalable simulation of coupled stochastic partial differential equations*, Comp. Phys. Comm. **184**, 201 (2013).

Supporting Information

Twist of generalized skyrmions and spin vortices in a polariton superfluid

SI Text

Experimental methods. The experimental polariton device is an AlGaAs 2λ microcavity with three 8 nm $\text{In}_{0.04}\text{Ga}_{0.96}\text{As}$ quantum wells. All the experiments shown here are performed at a temperature of 10 K in a region of the sample clean from defects. The excitation beam is a 4.0 ps Gaussian laser pulse with a repetition rate of 80 MHz selectively tuned on the lower polariton branch energy. Its intensity is adjusted so that to keep the resonantly excited fluid in a linear regime during the whole dynamics. In order to obtain the four different initial topological patterns (as reported in the table of Fig. 1M) we used a combination of impinging polarization, electrical tuning of the q -plate and waveplates as described below. In the case of the spin vortices the pulse is linearly polarized and the tuning of the q -plate is complete (100%). This allows to directly obtain a hedgehog pattern at the exit. Upon insertion of a half-wave plate (HWP) after the q -plate, we locally rotate the linear vectors of such pattern, obtaining the hyper-spin topology. In the case of the skyrmion, we send the pulse with a circular polarization onto the q -plate which is now partially tuned (50%). This results in an outgoing lemon skyrmion, which can be rotated by means of an HWP into its conjugated state, the star skyrmion.

On the detection side, to obtain polarization-resolved imaging, a waveplate and a linear polarizer are inserted before the charge coupled device. Upon using a HWP before the polarizer it is possible to resolve every direction of the linear polarization (H , V , D and A), while replacing the HWP with a quarter-wave plate is possible to map the circular polarizations (R and L). In this way we perform six dynamical sequences for each initial topology, from which it is possible to extract each independent degree of polarization. The three Stokes parameters are effectively derived as $S_1 = \frac{I_H - I_V}{I_H + I_V}$, $S_2 = \frac{I_D - I_A}{I_D + I_A}$ and $S_3 = \frac{I_R - I_L}{I_R + I_L}$, where the intensities are a function of both time and space [e.g., $I_H(x, y, t)$]. We checked that the total intensity in each of the three basis is the same at each point in space and time, $(I_H + I_V)(x, y, t) = (I_D + I_A)(x, y, t) = (I_R + I_L)(x, y, t)$. In other terms, that there is no significant depolarization and the six measurements are consistent with each other.

To obtain the time dynamics, the emission profiles are made to interfere with a delayed expanded reference beam carrying homogeneous density and phase profiles. Such technique is known as off-axis digital holography and relies on the use of Fast Fourier Transform (FFT) to filter only the information associated with the simultaneity between the emission and the delayed reference pulse. In this way it is possible to study the

dynamics of the polariton fluid, by obtaining the 2D real space snapshots of both the emission amplitude and phase, at a given time frame set by the delay. Each final snapshot results from thousands of repeated events, whose stability is based on the repeatability of the dynamics (with respect to the physics of the polaritons) and on the acquisition speed of each single interferogram (with respect to the experimental setup). Despite the fact that here we mostly used intensity features in each of the six pseudospin vectors, to study the polarization degree distribution and evolution it is also possible to look at the phase maps to devise the phase singularities at the cores of the vortex states (which here we did to check their stability in time). Additional details on the technique and the sample can be found in refs. 22, 30, and 33.

Theory models. In order to understand the physical origins of our observations, we perform numerical modelling of the system's dynamics using two-component open-dissipative Gross-Pitaevskii equations, which describe the microcavity photon field ϕ_{\pm} and the quantum well exciton field ψ_{\pm} coupled to each other:

$$\begin{aligned} i\hbar \frac{\partial \phi_{\pm}}{\partial t} &= \left(-\frac{\hbar^2}{2m_{\phi}} \nabla^2 - i\frac{\hbar}{2\tau_{\phi}} \right) \phi_{\pm} + \frac{\hbar\Omega_R}{2} \psi_{\pm} \\ + \chi \left(\frac{\partial}{\partial x} \mp i\frac{\partial}{\partial y} \right)^2 \phi_{\mp} &+ \frac{1}{2}\chi_0 \phi_{\mp} + D\phi_{\pm} + F_{\pm} \quad (S1) \\ i\hbar \frac{\partial \psi_{\pm}}{\partial t} &= \left(-\frac{\hbar^2}{2m_{\psi}} \nabla^2 - i\frac{\hbar}{2\tau_{\psi}} \right) \psi_{\pm} + \frac{\hbar\Omega_R}{2} \phi_{\pm} \\ &+ \alpha_1 |\psi_{\pm}|^2 \psi_{\pm} + \alpha_2 |\psi_{\mp}|^2 \psi_{\pm}. \end{aligned}$$

Here the upper lines of both equations represent analogous terms for the two fields, which are the kinetic energy, the decay time and the Rabi coupling strength between photons and excitons, respectively. In practical terms, excitons have an effective mass m_{ψ} of 4-5 orders of magnitude greater than that of the microcavity photons m_{ϕ} , resulting in their kinetic energy being negligible. The exciton and photon lifetimes are $\tau_{\psi} = 1000$ ps and $\tau_{\phi} = 5$ ps, respectively, giving the lower polariton lifetime of $\tau_{LP} \approx 10$ ps at zero detuning and $k = 0$. The Rabi coupling is $\hbar\Omega_R = 5.3$ meV. Selective excitation of the LPB can be obtained by using ps pulses with less than 1 meV energy width, tuned on the lower polariton mode as in the experiments. The bottom lines in both equations represent the specific terms acting on the two fields. The exciton-exciton interaction strengths used in the simulations are $\alpha_1 = +2 \mu\text{eV} \cdot \mu\text{m}^2$ for the intra-spin nonlinearities and $\alpha_2 = -0.2 \mu\text{eV} \cdot \mu\text{m}^2$ for the inter-spin ones (34). However, in the present work we are interested in the linear regime and specifically in the terms directly acting on the photonic fields, as discussed in the following.

The photonic linear coupling between different polarizations is given by the finite- k TE-TM splitting term χ and the k -independent anisotropy splitting χ_0 . The former appears due to the difference of transverse-electric and transverse-magnetic masses of microcavity

modes (35) as $\chi = \frac{\hbar^2}{4} \left(\frac{1}{m_\phi^{\text{TE}}} - \frac{1}{m_\phi^{\text{TM}}} \right)$, where the two effective masses imbalance is assumed $m_\phi^{\text{TE}}/m_\phi^{\text{TM}} = 0.95$ in our case. The k -independent splitting χ_0 between linearly polarized modes, which is due to strain effects (36, 37) and heavy-light hole mixing (38) on the quantum well interfaces, results in a different energy shift between the relevant linear polarized modes, and in the accumulation of a relative phase. In our simulations, we assumed xy directions for the anisotropy axis, and used 4 different χ_0 values ($\chi_{01} = 0.01$ meV, $\chi_{02} = 0.02$ meV, $\chi_{03} = 0.03$ meV, $\chi_{04} = 0.04$ meV).

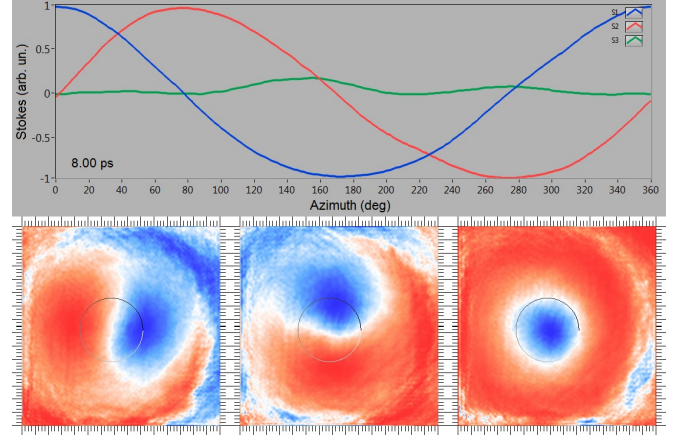
The disorder potential term $D(x, y)$, produced by the inhomogeneities inside the cavity mirror, which is reported here only for completeness, was not used and not needed to reproduce the observed dynamics. Finally, the initial laser pulse is described as a pulsed Laguerre-Gauss F_\pm :

$$F_\pm(\mathbf{r}) = f_\pm r^{|l_\pm|} e^{-\frac{1}{2} \frac{r^2}{\sigma_r^2}} e^{il_\pm \theta} e^{-\frac{1}{2} \frac{(t-t_0)^2}{\sigma_t^2}} e^{i(\mathbf{k}_p \cdot \mathbf{r} - \omega_p t)}$$

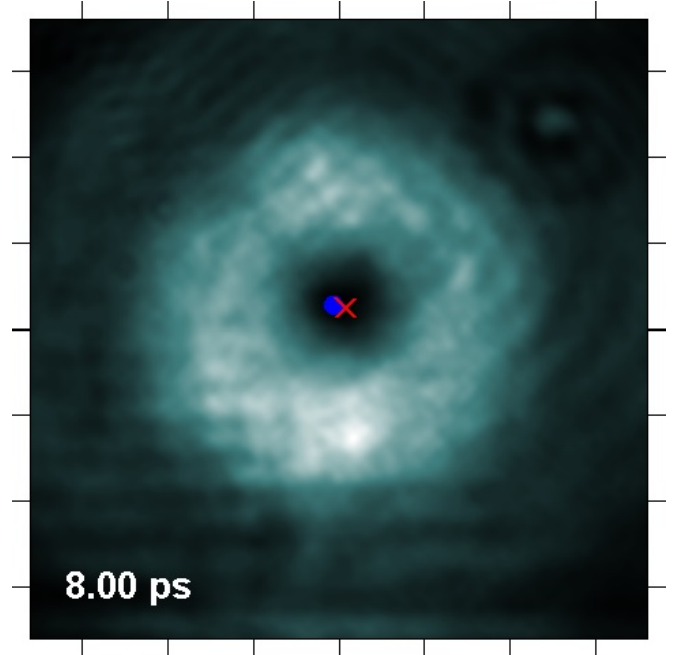
with a winding number of the vortex state in the σ_\pm component represented by l_\pm , and a strength f that reproduces the total number of output photons. The parameters of the initial state are chosen to reproduce the experimental specifics (σ_r and σ_t resulting in space and time FWHM equal to 30 μm and 4 ps, respectively). The initial state is centered on the LPB mode at 836 nm and at $\mathbf{k}_p = 0$.

Computational methods. The dynamics of equation S1 is simulated using the XMDS2 software framework (40). We employed adaptive step-size algorithm based on fourth and fifth order “embedded Runge-Kutta” (ARK45) method with periodic boundary conditions. This algorithm was also tested against eighth and ninth order (ARK89) of “embedded Runge-Kutta” method. The periodic boundary condition is an artefact of using FFT in order to efficiently switch between the real space to compute the potential energy and the momentum space to evaluate the kinetic energy. This method ensures very fast computation of each time step. In order to ensure that all flux leaving the system is not coming back from the other side due to the periodic boundary conditions, we implemented additional circular/ring absorbing boundary conditions, with the depth and the width carefully adjusted to the geometry of current experiments. We solve the equations on a 2D finite grid of $N \times N = 1024 \times 1024$ points and lattice spacing $l = 0.54 \mu\text{m}$ in a box of $L \times L = 556 \times 556 \mu\text{m}^2$. The large size of the simulation box ensures that polariton density drops practically to zero at the boundary. However, in all the maps we plot the physically relevant central region only, where the density of polaritons is still significant.

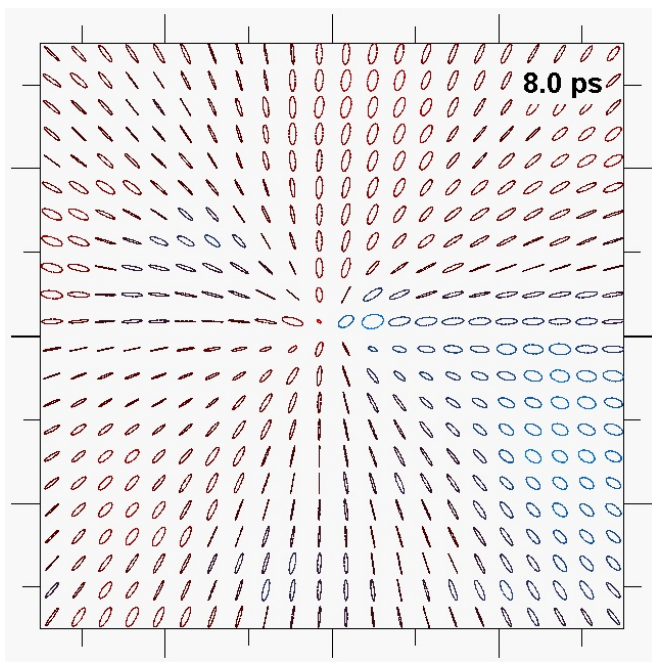
SI Movies



Movie S1: Lemon skyrmion, dynamics of the $S_{1,2,3}$ Stokes maps on a $90 \times 90 \mu\text{m}^2$ wide area and with time step of 0.5 ps. The top line shows the associated azimuthal profiles computed along the real-space circle represented in the maps, as in the case of Fig. 2E-H. The initially flat profile of the S_3 circular degree of polarization grows in time assuming a sinusoidal modulation as large as the other two Stokes parameters. [Movie S1](#)

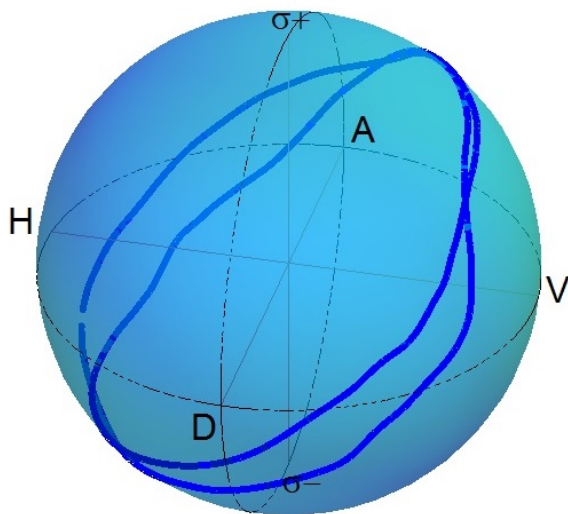


Movie S2: Hedgehog vortex, dynamics of the total polariton density distribution on a $72 \times 72 \mu\text{m}^2$ area. The associated positions of the counter-winding phase singularities in the two spin components are represented too, to show their fundamental stability over the whole dynamics (blue dot corresponds to the σ_+ and red cross to the σ_- spin population). [Movie S2](#)

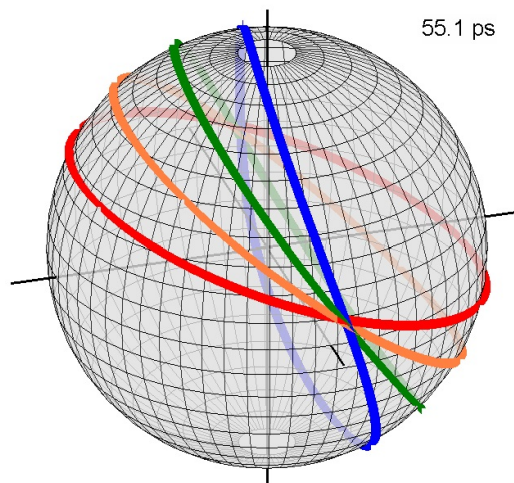


Movie S3: Representation of the polarization texture of the hedgehog vortex and of its reshaping dynamics over a $70 \times 70 \mu\text{m}^2$ wide area. The initially radial field evolves in time assuming an elliptical polarization degree with a four-sectors configuration. [Movie S3](#)

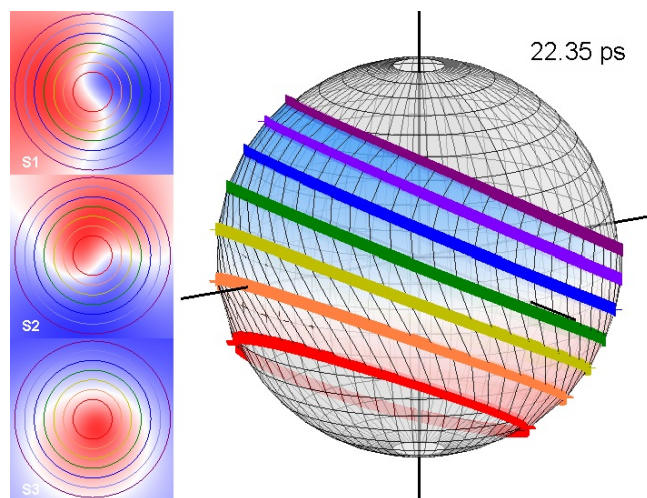
60.0 ps



Movie S4: The dynamics of the hedgehog vortex represented by means of its mapping onto the Poincaré sphere. The action of xy anisotropy produces a twist of the pseudospin double-loop plane towards the poles of the sphere. [Movie S4](#)



Movie S5: Numerical model dynamics of the lemon skyrmion twist, plotted on the Poincaré sphere. Each twisting loop corresponds to a different value of the anisotropy ($\chi_{01}, \chi_{02}, \chi_{03}, \chi_{04}$) consistently to what reported in Fig. 4N,O. [Movie S5](#)



Movie S6: Numerical star skyrmion twist for a value of the anisotropy χ_{04} . The $S_{1,2,3}$ Stokes degree of polarizations are plotted in the left panels over a $60 \times 60 \mu\text{m}^2$ area. Several concentric circles in real space (each represented with a different color) are conformally mapped onto the Poincaré sphere on the right panel (the l -line corresponds to the green color curve). The dynamical twist is similar for each circle, highlighting the generalized skyrmion features. At around 65 ps the twist angle has reached 90° and the S_2 and S_3 distributions in real space have roughly swapped with respect to initial time. Upon longer time the twist leads to a complete reversal of the initial star skyrmion into its conjugate state, the lemon skyrmion. [Movie S6](#)